Thursday, 2 May 2024, Lloret del Mar, Spain

Refining techniques and developments

Franck Pigeonneau
Mines Paris | PSL Univ. - Centre of Materials Forming, CNRS UMR 7635, Sophia Antipolis, France

1. Chemical engineering point of view

- Glass bath is an **open** reactor system.
- Existence of a residence time distribution $E(t)$.

Arbitrary reactor

$E(t) \sim$ probability density function:

$$\int_0^\infty E(t)dt = 1, \qquad (1)$$

$$\langle t \rangle = \int_0^\infty tE(t)dt. \qquad (2)$$

1. Chemical engineering point of view

- Glass bath is an **open** reactor system.
- Existence of a residence time distribution $E(t)$.

Arbitrary reactor

Plug flow reactor

$E(t) \sim$ probability density function:

$$\int_0^\infty E(t)dt = 1, \qquad (1)$$

$$\langle t \rangle = \int_0^\infty tE(t)dt. \qquad (2)$$

$$E(t) = \delta(t - t_s). \qquad (3)$$

1. Chemical engineering point of view

- Glass bath is an **open** reactor system.
- Existence of a residence time distribution $E(t)$.

Arbitrary reactor

Plug flow reactor

Continuous Stirred Tank Reactor

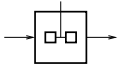

$E(t) \sim$ probability density function:

$$\int_0^\infty E(t)dt = 1, \qquad (1)$$

$$\langle t \rangle = \int_0^\infty tE(t)dt. \qquad (2)$$

$$E(t) = \delta(t - t_s). \qquad (3)$$

$$E(t) = \frac{e^{-t/t_s}}{t_s}. \qquad (4)$$

1. Chemical engineering point of view

- Glass bath is an **open** reactor system.
- Existence of a residence time distribution $E(t)$.

Arbitrary reactor

Plug flow reactor

Continuous Stirred Tank Reactor

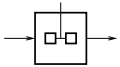

$E(t) \sim$ probability density function:

$$\int_0^\infty E(t)dt = 1, \qquad (1)$$

$$\langle t \rangle = \int_0^\infty tE(t)dt. \qquad (2)$$

$$E(t) = \delta(t - t_s). \qquad (3)$$

$$E(t) = \frac{e^{-t/t_s}}{t_s}. \qquad (4)$$

$$t_s = \frac{m}{\dot{m}}: \textbf{ Space time}. \qquad (5)$$

t_s is useful to normalise t and $E(t)$

$$\bar{t} = \frac{t}{t_s}, \ \bar{E}(\bar{t}) = t_s E(t). \qquad (6)$$

1. Chemical engineering point of view

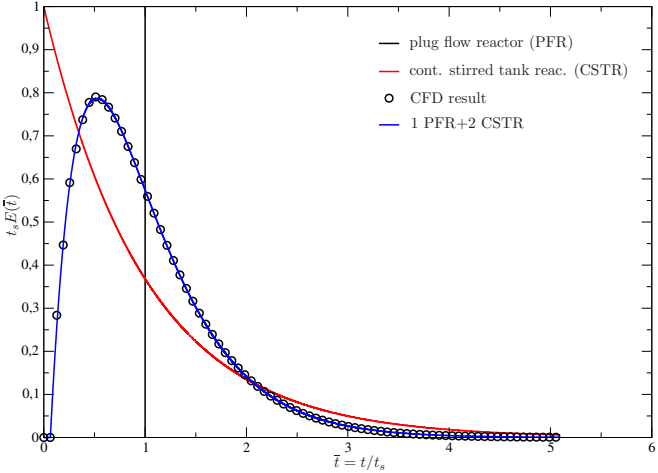

Figure 1: Residence time distribution of PFR, CSTR and industrial glass furnace.

1. Chemical engineering point of view

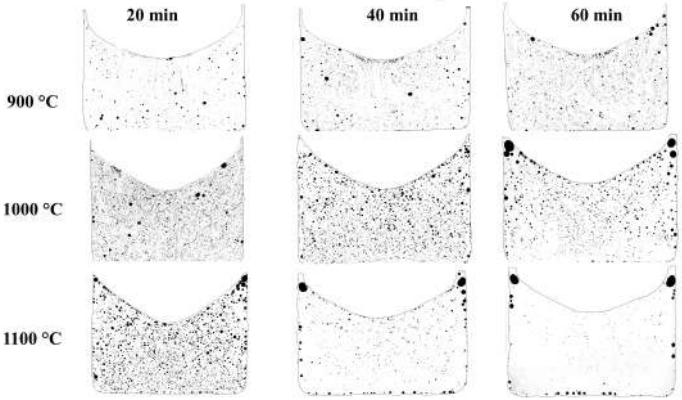

Figure 2: Bubble population in borosilicate liquid from post-mortem analysis[1].

[1] L. Pereira et al.: Experimental study of bubble formation in a glass-forming liquid doped with cerium oxide, in: J. Am. Ceram. Soc. 103 (2020), pp. 2453–2462.

1. Chemical engineering point of view

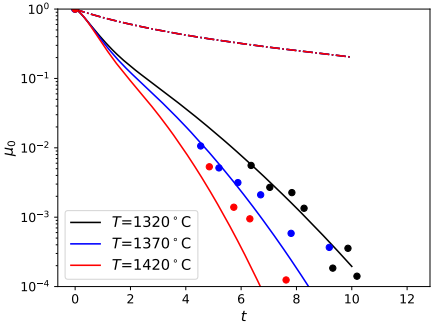

Figure 3: $\mu_0 = N(t)$ vs. t for T=1320, 1370 and 1420 °C[2]. Solid circles from Bastick[3].

$$N(t) = N_0 e^{-\alpha t}, \;\; N_0 \approx 10^8\,\mathrm{m}^{-3}. \tag{7}$$

[2] F. Pigeonneau/L. Pereira/A. Laplace: Dynamics of rising bubble population undergoing mass transfer and coalescence in highly viscous liquid, in: Chem. Eng. J. 455.2 (2023), p. 140920.

[3] R. E. Bastick: Laboratory experiments on the refining of glass, in: Symposium sur l'affinage du verre, Paris 1956, pp. 127–138.

1. Chemical engineering point of view

- In close reactor, **degree of conversion**:

$$X_{CR}(t) = 1 - \frac{N(t)}{N_0} = 1 - e^{-\alpha t}. \tag{8}$$

- In open reactor, the degree of conversion is given by[4]:

$$X_{OR} = \int_0^\infty X_{CR}(t)E(t)dt = 1 - G(\alpha), \tag{9}$$

$$G(\alpha) = \int_0^\infty E(t)e^{-\alpha t}dt, \text{ Laplace transformation.} \tag{10}$$

[4] J. Villermaux: Génie de la réaction chimique, Paris 1993.

1. Chemical engineering point of view

- Flat glass: less than 1 bubble of 200 µm/20 m^2 ➽ 10 bubbles/m^3:

$$G(\alpha) = 1 - X_{OR}(\alpha) = 10^{-7}. \tag{11}$$

- Container glass: less than 1 bubble/bottle ➽ 10^4 bubbles/m^3:

$$G(\alpha) = 1 - X_{OR}(\alpha) = 10^{-4}. \tag{12}$$

- According to Bastick[5], for T=1350 °C:

$$\alpha \approx 5 \cdot 10^{-4}\ \mathrm{s}^{-1}. \tag{13}$$

[5] Bastick: Laboratory experiments on the refining of glass (see n. 3).

1. Chemical engineering point of view

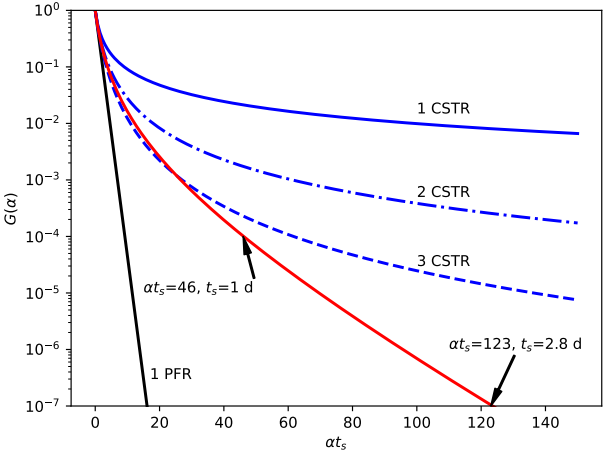

Figure 4: $G(\alpha) = 1 - X(\alpha)$ vs. αt_s for PFR, CSTR and industrial glass furnace.

1. Chemical engineering point of view

According to Pereira et al.[6]:

$$\alpha \sim \frac{\rho g a^2}{\eta(T)H}$$

[6] Pereira et al.: Experimental study of bubble formation in a glass-forming liquid doped with cerium oxide (see n. 1).

1. Chemical engineering point of view

According to Pereira et al. :

$\nearrow a \Rightarrow$ chemistry, $\searrow P$[6]

$$\alpha \sim \frac{\rho g a^2}{\eta(T) H}$$

[6] G. E. Kunkle/W. M. Welton/R. L. Schwenninger: Melting and vacuum refining of glass or the like and composition of sheet, US Patent 4,738,938, PPG Industries, Inc., 1988.

1. Chemical engineering point of view

According to Pereira et al. :

$$\nearrow a \Rightarrow \text{chemistry}, \searrow P$$

$$\alpha \sim \frac{\rho g a^2}{\eta(T) H}$$

$$\nearrow T \Rightarrow \searrow \eta$$

1. Chemical engineering point of view

According to Pereira et al. :

$$\nearrow g \Rrightarrow \text{centrifugal fining}^{6} \qquad \nearrow a \Rrightarrow \text{chemistry}, \searrow P$$

$$\alpha \sim \frac{\rho g a^2}{\eta(T)H}$$

$$\nearrow T \Rrightarrow \searrow \eta$$

[6] J. Ferguson: Centrifugal glass-melting furnace, US Patent 2,006,947, 1930.

1. Chemical engineering point of view

According to Pereira et al. :

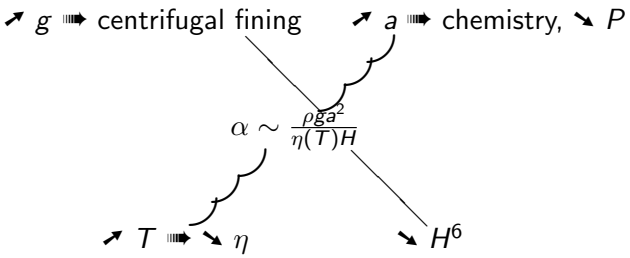

[6] P. Jeanvoine et al.: Procédé et dispositif de fusion et d'affinage de matières vitrifiables, Eur. Patent 0 970 021 B1, Saint-Gobain Glass France, 2005.

2. Mass transfer around a bubble

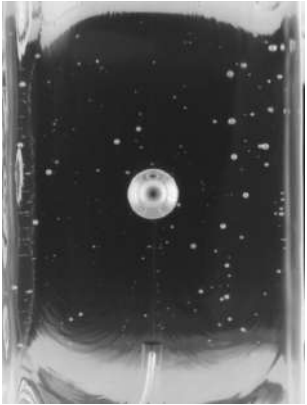

2. Mass transfer around a bubble

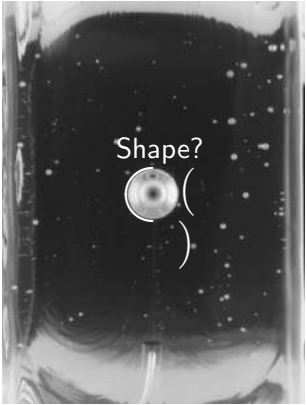

2. Mass transfer around a bubble

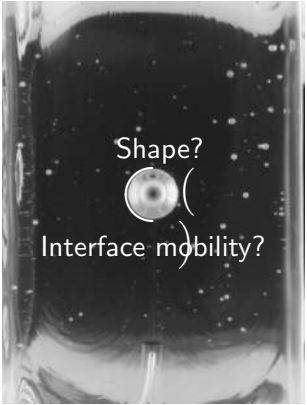

2. Mass transfer around a bubble

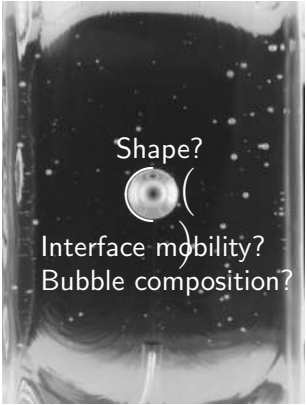

2. Mass transfer around a bubble

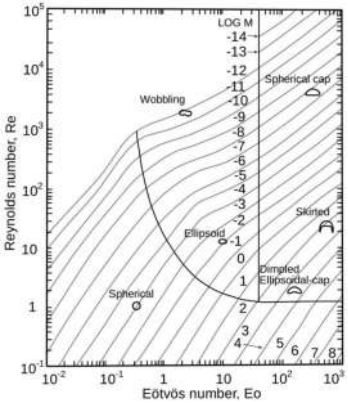

$$\mathrm{Eo} = \mathrm{Bo} = \frac{\rho g D^2}{\gamma}$$

$$\mathrm{Re} = \frac{\rho U D}{\eta}$$

$$\mathrm{Mo} = \frac{g \eta^4}{\rho \gamma^2}$$

Figure 5: $\mathrm{Eo} - \mathrm{Re}$ diagram[7].

[7] R. Clift/J. R. Grace/M. E. Weber: Bubbles, Drops, and Particles, New York 1978.

2. Mass transfer around a bubble

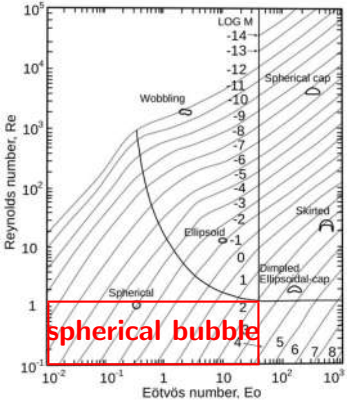

$$\mathrm{Eo} = \mathrm{Bo} = \frac{\rho g D^2}{\gamma} < 40$$

$$\mathrm{Re} = \frac{\rho U D}{\eta} < 1$$

$$\mathrm{Mo} = \frac{g\eta^4}{\rho\gamma^2} \approx 3 \times 10^2$$

Figure 5: $\mathrm{Eo} - \mathrm{Re}$ diagram[7].

[7] Clift/Grace/Weber: Bubbles, Drops, and Particles (see n. 7).

2. Mass transfer around a bubble

Jucha et al.[8]

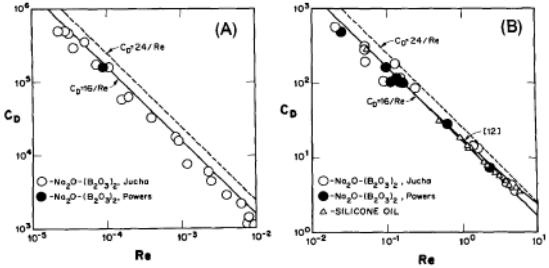

Hornyak & Weinberg[9]

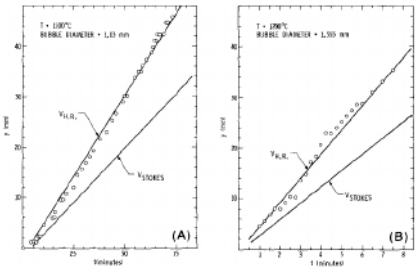

Figure 6: Drag law in glass forming liquids.

[8] R. B. Jucha et al.: Bubble rise in glassmelts, in: J. Am. Ceram. Soc. 65 (1982), pp. 289–292.

[9] E. J. Hornyak/M. C. Weinberg: Velocity of a freely rising gas bubble in a soda-lime silicate glass melt, in: J. Am. Ceram. Soc. 67 (1984), pp. C244–C246.

2. Mass transfer around a bubble

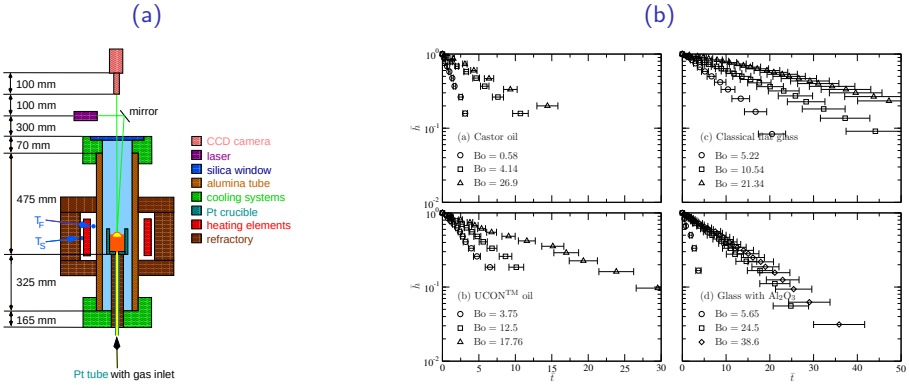

Figure 7: Film drainage at a free surface of high viscous liquids[10]: (a) expe. setup, (b) $\overline{h}$ vs. $\overline{t}$.

[10] H. Kočárková/F. Rouyer/F. Pigeonneau: Film drainage of viscous liquid on top of bare bubble: Influence of the Bond number, in: Phys. Fluids 25 (2013), p. 022105.

2. Mass transfer around a bubble

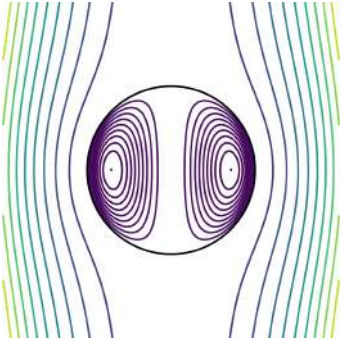

Figure 8: Stream functions inside and outside of a rising bubble.

According to Hadamard[a] & Rybczynski[b]:

$$\mathbf{F} = -4\pi\eta a(\mathbf{V} - \mathbf{U}), \qquad (14)$$

$$\mathbf{V} = -\frac{\rho \mathbf{g} a^2}{3\eta}. \qquad (15)$$

[a] J. Hadamard: Mouvement permanent lent d'une sphére liquide et visqueuse dans un liquide visqueux, in: C. R. Acad. Sci. Paris 152 (1911), pp. 1735–1738.

[b] W. Rybczynski: Uber die fortschreitende bewegun einer flussingen kugel in einem zaben medium, in: Bull. de l'Acad. des Sci. de Cracovie, série A 1 (1911), pp. 40–46.

2. Mass transfer around a bubble

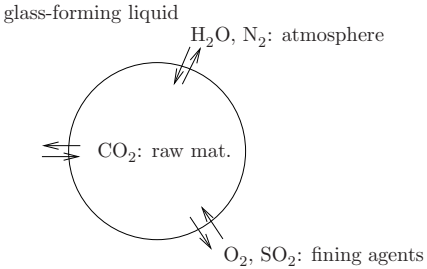

Figure 9: Gaseous species involved in mass transfer between bubbles and liquid.

$$\frac{dn_i}{dt} = \int_S \mathcal{D}_i \boldsymbol{\nabla} C_i \cdot \mathbf{n} dS = 4\pi a^2 \mathbf{J_i}, \quad (16)$$

$$\left[P_0 + \rho(H - z) + \frac{2\gamma}{a}\right] \frac{4\pi a^3}{3} = \left(\sum_{i=1}^{N} n_i\right) \mathcal{R}T, \quad (17)$$

$$\frac{d\mathbf{x}}{dt} = \mathbf{u} - \frac{\rho \mathbf{g} a^2}{3\eta}. \quad (18)$$

2. Mass transfer around a bubble

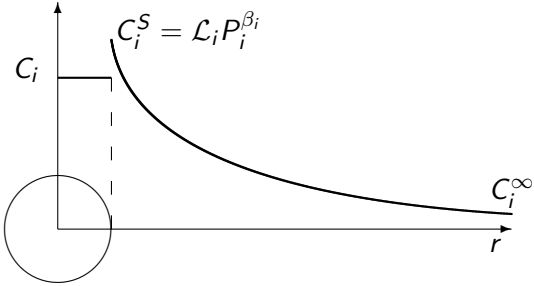

2. Mass transfer around a bubble

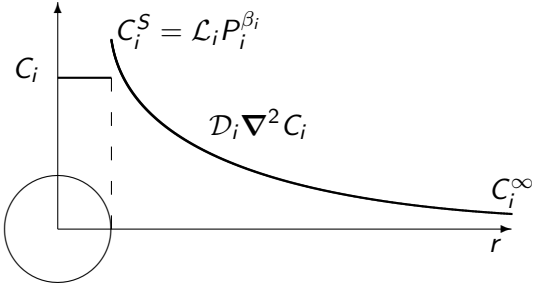

2. Mass transfer around a bubble

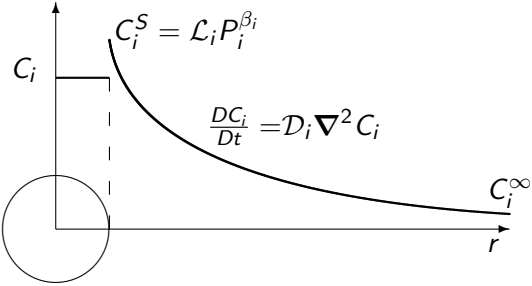

2. Mass transfer around a bubble

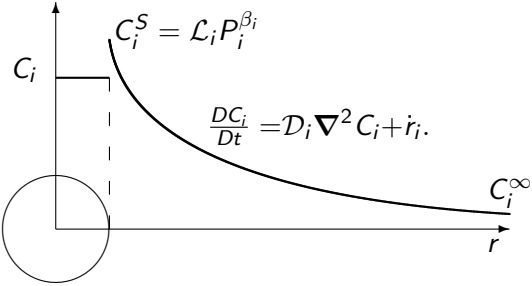

2. Mass transfer around a bubble

- Without convection and in steady-state regime:

$$\frac{d}{dr}\left(r^2\frac{dC_i}{dr}\right) = 0, \tag{19}$$

$$C_i(r) = C_i^\infty - \frac{(C_i^\infty - C_i^s)a}{r}, \tag{20}$$

$$J_i = \frac{\mathcal{D}_i(C_i^\infty - C_i^s)}{a}. \tag{21}$$

2. Mass transfer around a bubble

In the case of a rising bubble, the problem is normalised:

$$\bar{\mathbf{x}} = \frac{\mathbf{x}}{2a}, \quad \bar{C}_i = \frac{C_i - C_i^{\infty}}{C_i^s - C_i^{\infty}}. \tag{22}$$

In steady-state and in spherical coordinate system:

$$\left[\bar{u}_r \frac{\partial \bar{C}_i}{\partial \bar{r}} + \frac{\bar{u}_\theta}{\bar{r}} \frac{\partial \bar{C}_i}{\partial \theta}\right] = \frac{1}{\mathrm{Pe}_i\, \bar{r}^2} \left[\frac{\partial}{\partial \bar{r}}\left(\bar{r}^2 \frac{\partial \bar{C}_i}{\partial \bar{r}}\right) + \frac{1}{\sin\theta} \frac{\partial}{\partial \theta}\left(\sin\theta \frac{\partial \bar{C}_i}{\partial \theta}\right)\right], \tag{23}$$

$$\mathrm{Pe}_i = \frac{V_T 2a}{\mathcal{D}_i}. \tag{24}$$

2. Mass transfer around a bubble

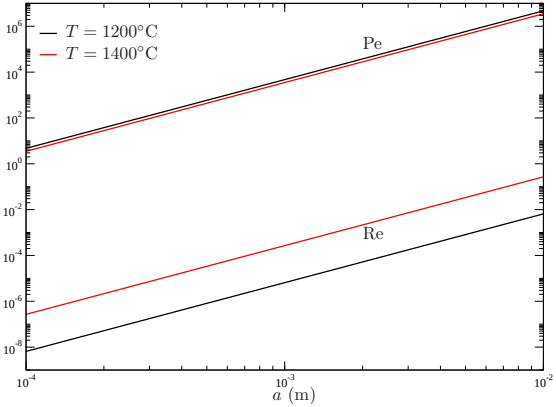

Figure 10: Re & Pe vs. a (m).

2. Mass transfer around a bubble

(a) Num. example

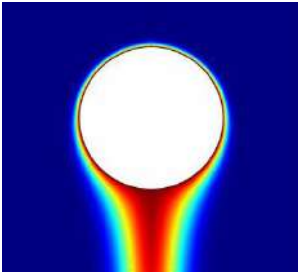

(b) Stretched coordinate[a]: $r = [1 + \delta(\mathrm{Pe}_i)\zeta]/2$

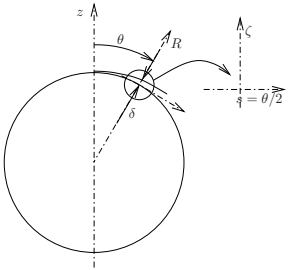

[a] E. J. Hinch: Perturbation Methods, 1991.

Figure 11: Chemical boundary layer around a rising bubble.

2. Mass transfer around a bubble

$$\left(\frac{\bar{u}_r}{\delta}\frac{\partial \bar{C}_i}{\partial \zeta} + \frac{\bar{u}_\theta}{1+\delta\zeta}\frac{\partial \bar{C}_i}{\partial \theta}\right) = \frac{1}{2\,\mathrm{Pe}_i\,\delta^2(1+\delta\zeta)^2}\left\{\frac{\partial}{\partial \zeta}\left[(1+\delta\zeta)^2\frac{\partial \bar{C}_i}{\partial \zeta}\right] + \frac{4\delta^2}{\sin\theta}\frac{\partial}{\partial \theta}\left(\sin\theta\frac{\partial \bar{C}_i}{\partial \theta}\right)\right\} \quad (25)$$

$$\frac{\bar{u}_r}{\delta} = -\frac{\cos\theta}{2}\left[\frac{2\zeta}{1+\hat{\eta}} + \frac{3\hat{\eta}-2}{2(1+\hat{\eta})}\delta\zeta^2 + \mathcal{O}(\delta^2)\right], \quad (26)$$

$$\frac{\bar{u}_\theta}{1+\delta\zeta} = -\frac{\sin\theta}{4}\left[-\frac{2}{1+\hat{\eta}} - \frac{4+10\hat{\eta}}{1+\hat{\eta}}\delta\zeta + \frac{6+19\hat{\eta}}{1+\hat{\eta}}\delta^2\zeta^2 + \mathcal{O}(\delta^3)\right]. \quad (27)$$

From the *principle of least degeneracy*[11]:

For solid particle or immobile interface ➽ $\hat{\eta} \to \infty$:

$$\delta \propto 1/\sqrt[3]{\mathrm{Pe}_i}. \quad (28)$$

For bubble ➽ $\hat{\eta} \to 0$:

$$\delta \propto 1/\sqrt{\mathrm{Pe}_i}. \quad (29)$$

[11] M. Van Dyke: Perturbation methods in fluid mechanics, Stanford, California 1975.

2. Mass transfer around a bubble

The molar flux becomes:

$$\frac{dn_i}{dt} = 4\pi a^2 J_i, \tag{30}$$

$$J_i = \frac{(C_i^s - C_i^\infty)\mathcal{D}_i}{2a}\,\mathrm{Sh}_i, \text{ without motion } \mathrm{Sh}_i = 2. \tag{31}$$

$$\mathrm{Sh}_i = \frac{2a}{\pi\delta}\int_S \frac{\partial \bar{C}}{\partial n} dS, \text{ **Sherwood** number.} \tag{32}$$

Levich's solution[12]:

$$\mathrm{Sh}_i = 0.991\sqrt[3]{\mathrm{Pe}_i}. \tag{33}$$

$$\mathrm{Sh}_i = 0.651\sqrt{\mathrm{Pe}_i}. \tag{34}$$

[12] V. G. Levich: Physicochemical hydrodynamics, Englewood Cliffs, N.J. 1962.

2. Mass transfer around a bubble

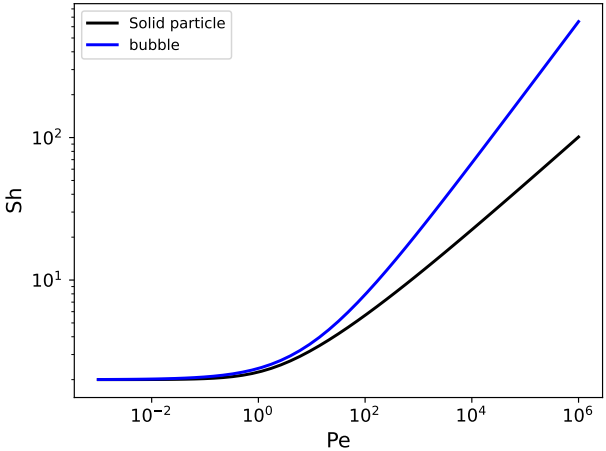

Figure 12: Sh vs. Pe for solid particle and bubble[13].

[13] Clift/Grace/Weber: Bubbles, Drops, and Particles (see n. 7).

2. Mass transfer around a bubble

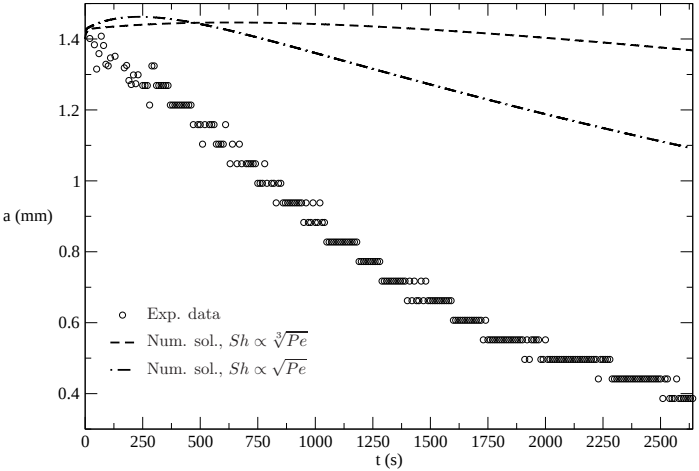

Figure 13: a vs. t of O_2 bubble at T=1400 °C, C_{Fe}=2.8 × 10^{-2} wt%, $\mathcal{R}_{\mathrm{Fe}}$ =0.575.

2. Mass transfer around a bubble

- Solve the advection/diffusion/reaction equation:

$$\frac{DC_{\mathrm{O}_2}}{Dt} = \mathcal{D}_{\mathrm{O}_2} \boldsymbol{\nabla}^2 C_{\mathrm{O}_2} + \dot{r}_{\mathrm{O}_2}. \tag{35}$$

- Assumptions:
  - The flow around the bubble is in the Stokes regime.
  - Interface between the bubble and glass is fully mobile.
  - Oxidation-reduction reaction of iron oxide is in chemical equilibrium[14].
  - Diffusion of iron is assumed very low.

$$\dot{r}_{\mathrm{O}_2} = -\frac{C_{\mathrm{Fe}} K_{\mathrm{Fe}}}{16 C_{\mathrm{O}_2}^{3/4} (K_{\mathrm{Fe}} + C_{\mathrm{O}_2}^{1/4})^2} \frac{DC_{\mathrm{O}_2}}{Dt}. \tag{36}$$

[14] R. G. C. Beerkens/H. de Waal: Mechanism of oxygen diffusion in glassmelts containing variable-valence ions, in: J. Am. Ceram. Soc. 73 (1990), pp. 1857–1861; F. Pigeonneau: Mass transfer of a rising bubble in molten glass with instantaneous oxidation-reduction reaction, in: Chem. Eng. Sci. 64.13 (2009), pp. 3120–3129.

2. Mass transfer around a bubble

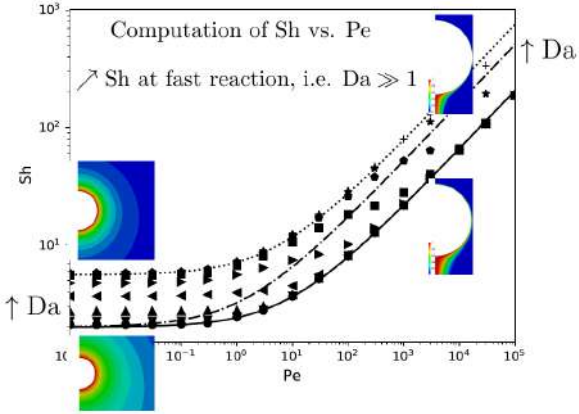

Figure 14: Sh vs. Pe for O_2[15].

[15] F. Pigeonneau/L. Pereira/A. Laplace: Mass transfer around a rising bubble in a glass-forming liquid involving oxidation-reduction reaction: Numerical computation of the Sherwood number, in: Chem. Eng. Sci. 232 (2021), p. 116382.

2. Mass transfer around a bubble

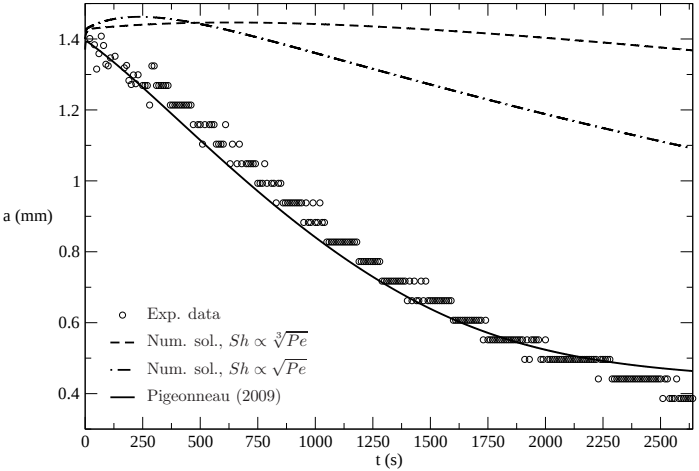

Figure 15: a vs. t of O_2 bubble at T=1400 °C, C_{Fe}=2.8 × 10^{-2} wt%, $\mathcal{R}_{\mathrm{Fe}}$ =0.575.

3. Fining process

3.1 Sulphate fining

$$\frac{dn_i}{dt} = 2\pi a \mathcal{D}_i \, \mathrm{Sh}_i \left(C_i^{\infty} - \mathcal{L}_i P_i^{\beta_i} \right), \tag{37}$$

$$\left[P_0 + \rho(H - z) + \frac{2\gamma}{a} \right] \frac{4\pi a^3}{3} = \left(\sum_{i=1}^{N} n_i \right) \mathcal{R} T, \tag{38}$$

$$\frac{d\mathbf{x}}{dt} = \mathbf{u} - \frac{\rho \mathbf{g} a^2}{3\eta}. \tag{39}$$

3. Fining process

3.1 Sulphate fining

$$\frac{dn_i}{dt} = 2\pi a \mathcal{D}_i \, \mathrm{Sh}_i \left(C_i^{\infty} - \mathcal{L}_i P_i^{\beta_i} \right), \tag{37}$$

$$\left[P_0 + \rho(H - z) + \frac{2\gamma}{a} \right] \frac{4\pi a^3}{3} = \left(\sum_{i=1}^{N} n_i \right) \mathcal{R} T, \tag{38}$$

$$\frac{d\mathbf{x}}{dt} = \mathbf{u} - \frac{\rho \mathbf{g} a^2}{3\eta}. \tag{39}$$

3. Fining process

3.1 Sulphate fining

- Multivalent elements oxidation-reduction state described by

$$\mathrm{M}^{(\mathrm{m+k})+}(l) + \frac{k}{2}\mathrm{O}^{2-}(l) \longleftrightarrow \mathrm{M}^{\mathrm{m}+}(l) + \frac{k}{4}\mathrm{O}_2(g), \tag{40}$$

$$\mathrm{SO_4}^{2+}(l) \longleftrightarrow \mathrm{SO}_2(g) + \frac{1}{2}\mathrm{O}_2(g) + \mathrm{O}^{2-}(l). \tag{41}$$

- Equilibrium with a gaseous atmosphere is given by

$$\mathrm{O}_2(g) \longleftrightarrow \mathrm{O}_2(l). \tag{42}$$

3. Fining process

3.1 Sulphate fining

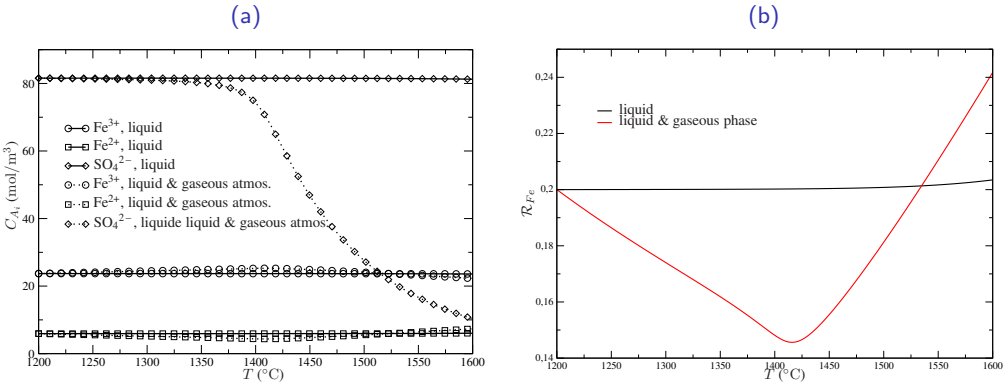

Figure 16: (a) Ion concentrations and (b) redox state $C_{Fe^{2+}}/C_{Fe}$ without and with thermodynamic equilibrium of gaseous phase.

3. Fining process

3.1 Sulphate fining

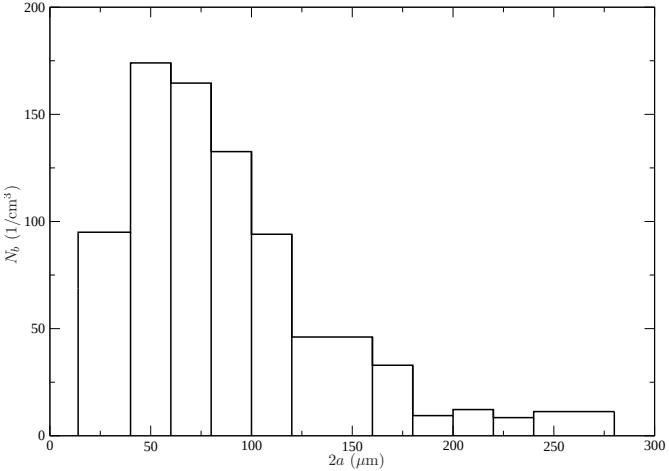

Figure 17: Bubble histogram vs. $2a$ [SGR, Paris, N. McDonald].

3. Fining process

3.1 Sulphate fining

Model coupling mass transfer between bubble and the liquid[16]:

$$\frac{dC_{A_i}}{dt} = \sum_{r=1}^{R} \nu_{ri} \frac{d\zeta_r}{dt}, \; i \in [1, N_l]. \quad (43)$$

$$\frac{dC_{G_j}}{dt} = \sum_{r=1}^{R} \beta_{rj} \frac{d\zeta_r}{dt} + S_{b,G_j}, \; j \in [1, N_{fg}], \quad (44)$$

$$\frac{dC_{G_j}}{dt} = S_{b,G_j}, \; j \in [N_{fg}+1; N_g]. \quad (45)$$

$$S_{b,G_j} = -4\pi \sum_{k=1}^{N_{c1}} a_k^2 k_{G_j,k} \left(C_{G_j} - \mathcal{L}_{G_j} P_{G_j,k}^{\alpha_{G_j}} \right) N_{b,k}, \quad (46)$$

$$\sum_{k=1}^{R} M_{rk} \frac{d\zeta_k}{dt} = \frac{d \ln K_r}{dT} \frac{dT}{dt} - \sum_{j=1}^{N_{fg}} \frac{\beta_{rj}}{C_{G_j}} S_{b,G_j}, \; r \in [1; R], \quad (47)$$

$$M_{rk} = \sum_{i=1}^{N_l} \frac{\nu_{ri}\nu_{ki}}{C_{A_i}} + \sum_{j=1}^{N_{fg}} \frac{\beta_{rj}\beta_{kj}}{C_{G_j}}. \quad (48)$$

[16] J. Kloužek et al.: The redox distribution at the interface of glass melts with different oxidation state, in: Ceram. Silik. 44 (2000), pp. 91–95; F. Pigeonneau: Coupled modelling of redox reactions and glass melt fining processes, in: Glass Technol.: Eur. J. Glass Sci. Technol. A 48.2 (2007), pp. 66–72.

3. Fining process

3.2 Water fining

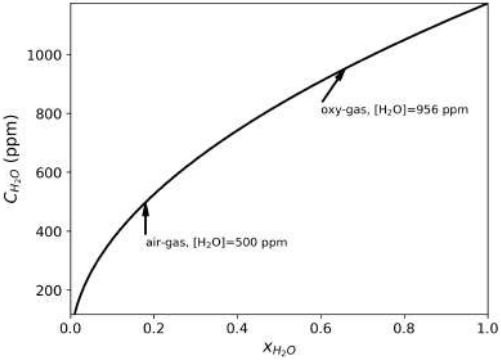

Figure 18: Amount of H_2O vs. x_{H_2O} with a solubility equal to $0.68e^{-613/T}$ at P=10^5 Pa according Beerkens[17].

[17] R. G. C. Beerkens: Analysis of advanced and fast fining processes for glass melts, in: Advances in Fusion and Processing of Glass III, New York 2004, pp. 3–24.

3. Fining process

3.2 Water fining

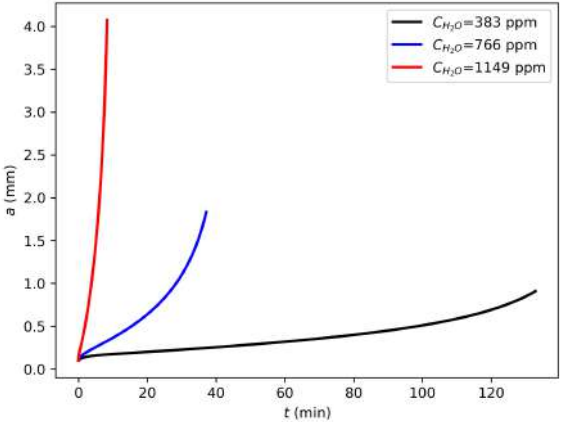

Figure 19: a vs. t with $a(0)=10^2$ µm and $T=1400\,^{\circ}$C.

3. Fining process

3.2 Water fining

- Patent proposed by Lazet[18].

Class	Ini. compo. ini.	N_b (m^{-3})	a_0 (mm)
1	CO_2	2.25×10^4	0.1
2	CO_2	2.25×10^4	0.25
3	CO_2	2.25×10^4	0.75
4	CO_2	2.25×10^4	1
5	H_2O	10^5	10

Table 1: Composition, volume concentration and initial radii of bubble classes.

[18] F. J. Lazet: Preparing alkali metal silicate glass with bubbles, US Patent 3,960,532 A, Philadelphia Quartz Company, 1975.

3. Fining process

3.2 Water fining

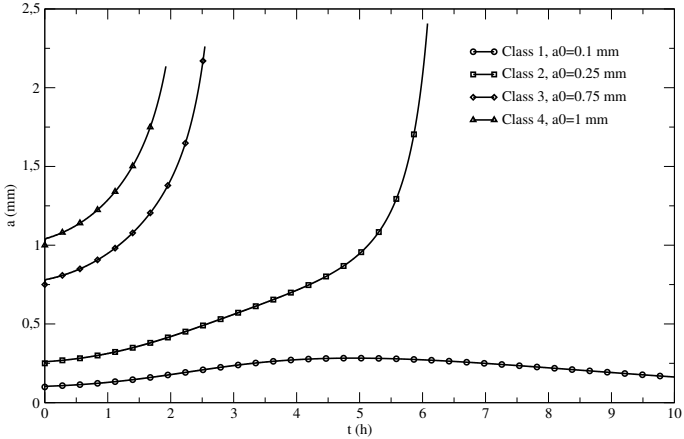

Figure 20: a vs. t for the 5 classes of bubbles at $T = 1200\,^{\circ}\mathrm{C}$.

3. Fining process

3.2 Water fining

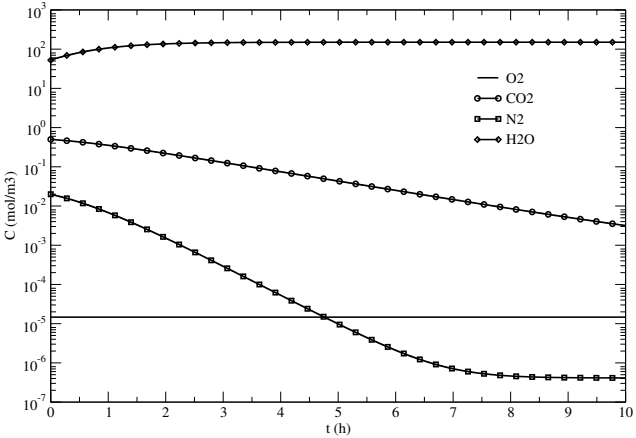

Figure 21: Molar concentration of dissolved gas in the liquid vs. t at T=1200 °C.

3. Fining process

3.3 Helium fining

- Patent proposed by Kobayashi et al.[19].
- He bubbling ➽ diffusion of He in the liquid ➽ migration of He in bubbles produced by the melting.
- Test with two populations of bubbles, one from melting with $10^8\,\mathrm{m}^{-3}$ and one due to the bubbling of He with $10^7\,\mathrm{m}^{-3}$ at $T = 1400\,^\circ\mathrm{C}$.
- Initial radius equal to $100\,\mu\mathrm{m}$.

[19] H. Kobayashi/S. E. Jaynes/R. G. C. Beerkens: Process of fining glassmelts using helium bubbles, US Patent 2006/0174655A1, Praxair, Inc., 2003.

3. Fining process

3.3 Helium fining

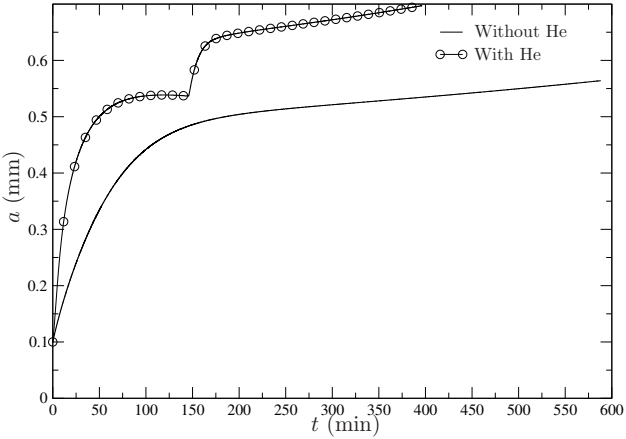

Figure 22: a vs. t for the 2 classes of bubbles at T=1400 °C.

3. Fining process

3.3 Helium fining

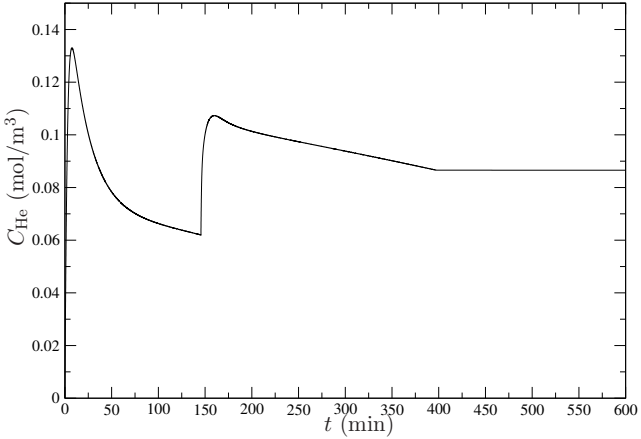

Figure 23: Molar concentration of He dissolved in the liquid vs. t at T=1400 °C.

3. Fining process

3.4 Centrifugal and low pressure fining

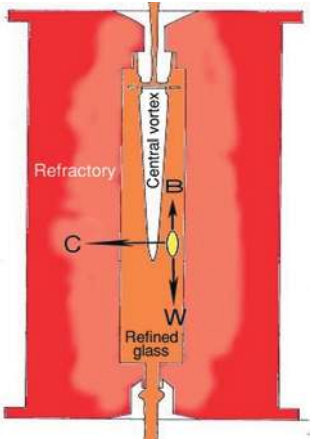

Figure 24: Centrifugal finer according to Spinosa[20].

[20] E. D. Spinosa: Modular refining methods, in: Am. Ceram. Soc. Bull. 83.10 (2004), pp. 25–27.

3. Fining process

3.4 Centrifugal and low pressure fining

- Tonarová et al.[21] provided an optimisation of the centrifugal fining.

$$P = P_0 + \rho g \left(H - \frac{\omega^2 R^2}{4g} - z \right) + \rho \frac{\omega^2 r^2}{2}. \tag{49}$$

[21] V. Tonarová/L. Němec/J. Kloužek: The optimal parameters of bubble centrifuging in glass melts, in: J. Non-Cryst. Solids 357 (2011), pp. 3785–3790.

3. Fining process

3.4 Centrifugal and low pressure fining

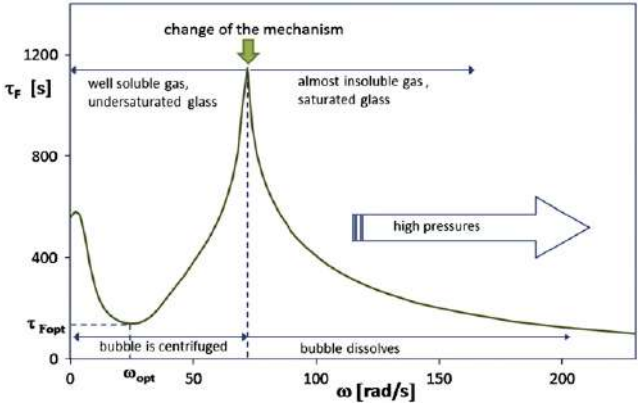

Figure 25: Fining time vs. ω according to Tonarová et al.[22].

[22] Tonarová/Němec/Kloužek: The optimal parameters of bubble centrifuging in glass melts (see n. 21).

3. Fining process

3.4 Centrifugal and low pressure fining

(a) P_{atm}=1 atm (b) P_{atm}=0.5 atm (c) P_{atm}=0.1 atm

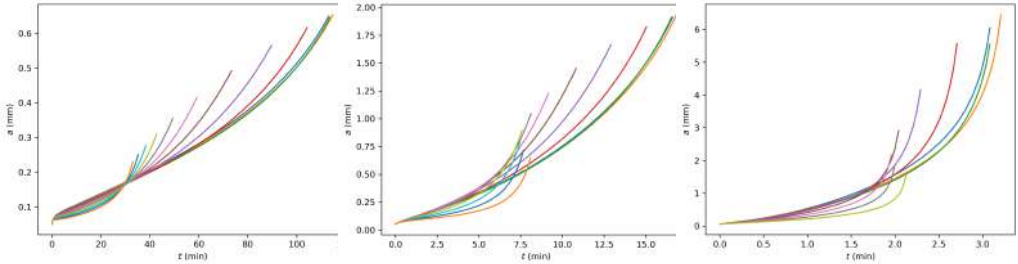

Figure 26: a vs. t for various ω for 3 atmospheric pressure.

3. Fining process

3.4 Centrifugal and low pressure fining

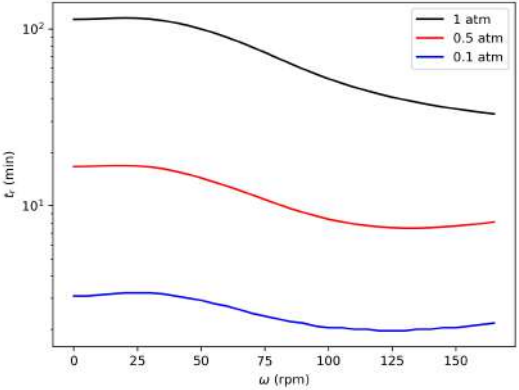

Figure 27: Fining time vs. ω for 3 atmospheric pressure.

4. Synthesis

Method	Structure	Installation	Operation	Development
Helium	Small	Familiar to industry	Complicated	Laboratory
Sonic	Small	Familiar to industry	Simple	Laboratory
Centrifugal	Large	Unfamiliar to industry	Extremely challenging	Pilot scale
Vacuum	Large	Unfamiliar to industry	Challenging	Commercial

Table 2: Comparison of refining methods[23].

[23] Spinosa: Modular refining methods (see n. 20).

4. Synthesis

Rapid melting
↓
Grain dissolution
↓
Alternative refining
↓
Less energy to product

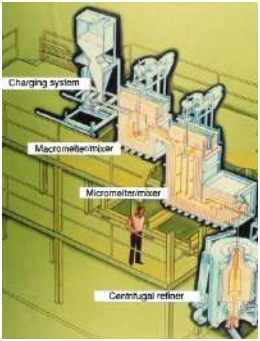

Figure 28: Segmented melter RAMAR of Owens-Illinois[a].

[a] F. G. Pellett et al.: Method for rapid melting and refining glass, US Patent 3,819,350, 1974.

Thank you all of you for your attention!

- Students:
  - H. Kočárková, M. Perrodin, M. Guémas, D. Boloré, L. Pereira.
- Colleagues:
  - **SGR, Paris**: M.-H. Chopinet, E. Gouillart, D. Martin, N. McDonald;
  - **Lab. Navier** (Univ. Paris-Est/Marne la Vallée): F. Rouyer;
  - **Lab. Génie Chim.** (Toulouse): P. Chamelot, O. Masbernat;
  - **I.M.F.T.** (Toulouse): E. Climent;
  - **LadHyX** (Ecole Polytechnique, Paris Saclay): A. Sellier;
  - **CEA Marcoule**: A. Laplace;
  - **Lab. Inorg. Mater.**, Univ. of Prague (Czech Republic): J. Kloužek.

Contact:

franck.pigeonneau@minesparis.psl.eu